agriculture

MDPI

Article

A Compliant Active Roller Gripper with High Positional Offset Tolerance for Delicate Spherical Fruit Handling

Haoran Zhu [1], Huanhuan Qin [2,*], Zicheng Qiu [2], Xinwen Chen [3], Jinlin Xue [1], Xingjian Gu [2] and Mingzhou Lu [2]

[1] College of Engineering, Nanjing Agricultural University, No. 666 Binjiang Avenue, Jiangbei New District, Nanjing 211800, China; zhrzip0201@163.com (H.Z.); xuejinlin@njau.edu.cn (J.X.)
[2] College of Artificial Intelligence, Nanjing Agricultural University, No. 666 Binjiang Avenue, Jiangbei New District, Nanjing 211800, China; qzcqzc99@163.com (Z.Q.); guxingjian@njau.edu.cn (X.G.); lmz@njau.edu.cn (M.L.)
[3] Institute of Animal Husbandry Quality Standards, Xinjiang Academy of Animal Science, No. 21, Karamay East Road, Sayibak District, Urumqi 830011, China; chenxinwen1123@outlook.com
* Correspondence: qhuanhuan1001@njau.edu.cn

Abstract: In the field of agricultural robotics, robotic grippers play an indispensable role, directly influencing the rate of fruit damage and handling efficiency. Currently, traditional agricultural robotic grippers face challenges such as high damage rates and high requirements for position control. A robotic gripper for stable spherical fruit handling with high positional offset tolerance and a low fruit damage rate is proposed in this paper. It adopts a three-finger structure. A flexible active roller is configured at the end of each finger, allowing fruit translation with just a gentle touch. An integrated pressure sensor within the active roller further enhances the gripper's compliance. To describe the effect of the gripper on the fruit, the interaction model was derived. Taking the tomato as a typical soft and fragile spherical fruit, three experiments were conducted to evaluate the performance of the proposed gripper. The experimental results demonstrated the handling capability of the gripper and the maximum graspable weight reached 2077 g. The average failure rate for the unilateral offset of 9 mm was only 1.33%, and for the bilateral offset of 6-6 mm was 4%, indicating the high positional offset tolerance performance and a low fruit damage rate of the gripper. The preliminary tomato-picking capability of the proposed gripper was also validated in a simplified laboratory scenario.

Keywords: robotic gripper; active roller; positional offset tolerance; force sensing; spherical fruit handling

Received: 1 December 2024
Revised: 24 December 2024
Accepted: 2 January 2025
Published: 20 January 2025

Citation: Zhu, H.; Qin, H.; Qiu, Z.; Chen, X.; Xue, J.; Gu, X.; Lu, M. A Compliant Active Roller Gripper with High Positional Offset Tolerance for Delicate Spherical Fruit Handling. *Agriculture* **2025**, *15*, 220. https:// doi.org/10.3390/agriculture15020220

1. Introduction

Fruits play an important role in human nutrition and health, especially as a source of vitamins, minerals, and dietary fiber [1]. The global production of fresh fruit has already reached 909.64 million metric tons in 2021. Currently, the scale of fruit cultivation and production is still on the rise. Agricultural product-handling robots have become an essential component of the fruit industry [2,3]. Robotic grippers (also called end-effectors) act as the terminal mechanisms of agricultural robots [4–7]. They directly interact with the fruits and their performance has a great influence on the handling efficiency and the fruit damage rate [8]. When handling delicate fruits, the grippers need to demonstrate high adaptability, flexibility, and precision to minimize damage to the products.

Rigid grippers are one of the most common grippers for fruit handling. They usually have rigid support structures with soft components (such as flexible membranes, rubbers,

etc.) attached to the inner surfaces to increase their compliance [9,10]. In the rigid grippers, servo-electric or pneumatic actuators drive two or more fingers to apply force constraints to the fruit. The typical interaction model between the rigid gripper and the spherical fruit is shown in Figure 1a. This type of interaction model is more common in force closure grasps. Force closure grasps typically rely on friction and utilize forces applied at contact points to resist any external wrench. The typical rigid grippers for fruit handling include a parallel two-finger gripper constructed by Festo [11], a robotic gripper module with 3D-printed fingers designed by Liu et al. [12], a gripper prototype based on the crank-slider mechanism proposed by Russo et al. [13], an underactuated tendon-driven end-effector with three identical fingers [14], and a rotational gripper with the spring tension structure designed by Yaguchi et al. [15]. The rigid grippers have advantages in terms of fast response and force controllability. However, considering the soft, fragile nature of most ripe fruits, the force applied to the fruits must be precisely controlled to ensure high compliance. Hence, force sensors are inevitably required, which makes the gripper complex and inaccessible. Another inherent disadvantage of the rigid grippers is their limited adaptability to the shapes and contours of fruits, potentially resulting in increased fruit damage or handling failures.

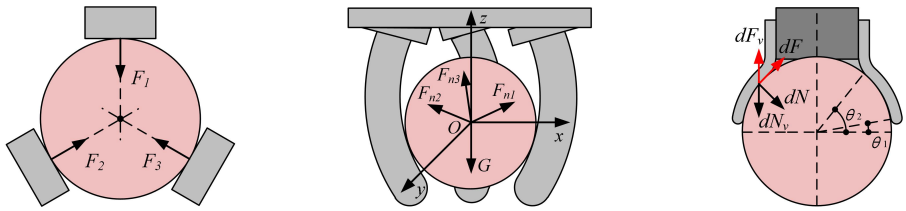

(**a**) (**b**) (**c**)

Figure 1. Typical interaction models between grippers and spherical fruits. Taking three-finger grippers as examples. F_1, F_2, and F_3 in (**a**) are forces exerted by three rigid fingers. F_{n1}, F_{n2}, and F_{n3} in (**b**) are resultant forces exerted by three soft fingers. dN and dF in (**c**) are the normal force and frictional force, dN_v and dF_v are their vertical components, and θ_1 and θ_2 represent lower and upper contact points. (**a**) Rigid gripper–fruit model. (**b**) Soft gripper–fruit model. (**c**) Vacuum suction gripper–fruit model.

Soft grippers are another common type of grippers mounted on the end of handling robots, capable of achieving conformal grasping in a non-destructive manner [16,17]. In the soft gripper, the actuator drives the fingers towards the fruit. Once in contact with the fruit, the fingers deform sufficiently to fit the surface of the fruit [18–20]. The typical interaction model between the soft gripper and the spherical fruit is shown in Figure 1b. This interaction model is more common in form closure grasps. Form closure grasps (also called enveloping grasps) typically impose kinematic constraints on objects and require more contact points than force closure grasps. Some representative soft grippers include a three-finger soft robotic gripper driven by the pneumatic actuators [21], a stiffness-tunable soft robotic gripper for dexterous grasping [22], a dual-mode soft gripper with a bend angle of 90° and a maximum lifting force of 1 N [23], a three-finger hybrid gripper with 2.56 N fingertip force [24], and a three-finger soft gripper with the Fin Ray structure [25]. Soft grippers show great potential in the pliable bending motion, inherent compliance, and a simple morphological structure. However, they still need to be improved in terms of robustness, control frequency, and sensing integration [26].

Other grippers for fruit handling mainly include vacuum grippers and grippers based on smart materials. The vacuum gripper (also known as the suction gripper) establishes a tight connection between the gripper and the fruit by utilizing a pressure difference (as shown in Figure 1c) [27], allowing for further manipulation of the fruit. Similar grippers include the 3D-printed soft suction gripper with an elastomer film for delicate fruit pick-

ing [28], the inherently gentle soft-touch gripper with a thin flexible latex membrane for fruit grasping [29], the vacuum-driven origami soft gripper with a flexible thin membrane for delicate food lifting [30], and the adaptive self-sealing suction robotic gripper with a thin flat elastic membrane for the pick-and-place task of apples and limes [31]. Vacuum grippers can handle many non-spherical fruits, as long as their surfaces are smooth. Furthermore, they are not sensitive to the location of the fruit, exhibiting low control complexity and high flexibility in path planning [32]. However, they are very sensitive to dusty conditions and require additional air pumps. The interference from adjacent fruits and branches can easily lead to grasping failure. The smart material-based gripper relies on the change of the material property (such as shape or yield stress) under the excitation of current, magnetic field, etc. The smart materials typically used in this type of gripper mainly include dielectric elastomers, electroadhesion, and magnetorheological fluid, etc. [33–38]. They show great potential in handling extremely fragile objects. However, their adoption in current fruit handling scenarios is difficult because they often have extremely high requirements for voltage, current, etc. Additionally, some of these materials, such as electroadhesion, require special surfaces to hold objects.

The comparison of the discussed grippers is shown in Table 1. They have shown great potential in the field of fruit grasping and even harvesting. However, most of them (especially rigid and soft grippers) are sensitive to the position of the target fruits; hence, the position of the grippers should be precisely controlled to successfully handle the fruits. In this paper, a compliant gripper with three active rollers to achieve high positional offset tolerance is proposed for handling spherical fruit. This gripper enables low damage rates and stable handling of the fruit by only touching it, without the need to precisely control the position of the gripper. With a flexible silicone membrane, the active roller facilitates the movement of the fruit into the gripper via friction force while ensuring the compliance of the gripper. An accessible pressure sensor is embedded into the active roller to measure the interaction force uniformly to further increase the compliance of the gripper. The main contributions of this paper are as follows: (1) a design methodology for an active roller gripper with high positional offset tolerance, (2) a derived interaction model to describe the effect of the gripper on the fruit, and (3) experimental verification of the proposed gripper.

Table 1. Comparison of discussed grippers.

Type		Typical Gripper	Target Object	Features
Rigid		Parallel two-finger gripper [11]	Apple	Adv. Fast response, force controllability Disad. Limited adaptability
		3D-printed two-finger gripper [12]	Orange	
		Three-finger robotic gripper [13]	Tomato	
Soft		Three-finger soft gripper [21]	Apple	Adv. Pliable bending motion, inherent compliance Disad. Low control frequency and robustness
		Three-finger hybrid gripper [24]	Apple	
		Three-finger soft gripper [25]	Apple	
Other	Vacuum	Vacuum suction gripper [28]	Pear	Adv. Limited fruit adaptability, low control complexity Disad. Sensitivity to dust, air pump requirement
		Vacuum-driven origami gripper [30]	Banana	
	Smart material	Soft compliant gripper [33]	Strawberry	Adv. Handling capability for fragile objects Disad. High requirements for voltage, current, etc.
		Magnetorheological gripper [35]	Orange	

The rest of this paper is organized as follows. The detailed mechanical design of the gripper and its force-sensing method is described in Section 2. The gripper–fruit interaction model is also presented in this section. Three experiments and the experimental results are described and discussed in Section 3. The conclusion and future work are given in Section 4.

2. Gripper Implementation

2.1. Mechanical Design

The general structure of the proposed gripper is shown in Figure 2. The gripper mainly includes a base, a soft support membrane, an embedded control unit, and three fingers. Each finger has two DoFs (Degrees of Freedom) and consists of a smart actuator, a link, and an active roller unit. The base is a two-layer structure with holes in the top layer to connect to the smart actuators and holes in the bottom layer for the robotic arm. The space between the two layers is used to place the embedded control unit. The smart actuators (XM430-W350-R, Dynamixel, Corona, CA, USA) with a gear ratio of 353.5 are adopted to drive the links through horns. The replaceable active roller units are located at the ends of the links for improved maintainability. With the cooperation of the smart actuators, links, and roller units, fruits can be handled smoothly. The membrane is molded using a silicone gel with Shore A Hardness 15. It is soft enough to support and constrain fruits of different sizes as they are fully translated into the gripper. The embedded control unit mainly includes a microcontroller (ATmega2560, Microchip, Chandler, AZ, USA), a power management module, a TTL to RS-485 interface module, and three DC motor drivers. The gripper can work properly when DC power (12 V) is applied.

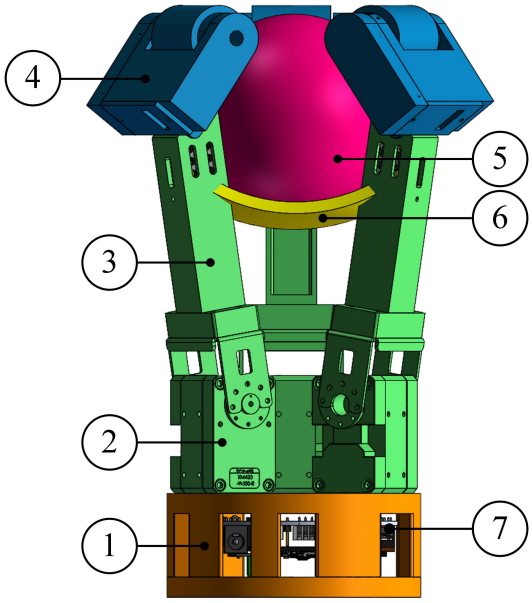

Figure 2. General mechanical assembly of gripper. (1) Base, (2) smart actuator, (3) link, (4) active roller unit, (5) spherical fruit, (6) soft membrane, and (7) embedded control unit.

The detailed structure of the active roller unit is displayed in Figure 3. A micro DC motor (GA12-N20, ASLONG, Shenzhen, China) with a gear ratio of 210 is used to drive the roller at a given speed. It is inserted into the unit body and fixed by the motor cover. A gear set is adopted for motion transmission, with one end connected to the motor and the other end connected to the spool connector. It is shielded by the unit side cover to reduce outside interference. The spool is inserted into the roller and fixed to the roller with glue. One end of it is connected to the spool connector, and the other end is fixed on the unit body through a bearing. A pressure sensor (MS5637, TE Connectivity, Tijuana, Mexico) is embedded within the roller to measure the interaction force uniformly. To prevent wires from getting tangled, a slip ring is installed.

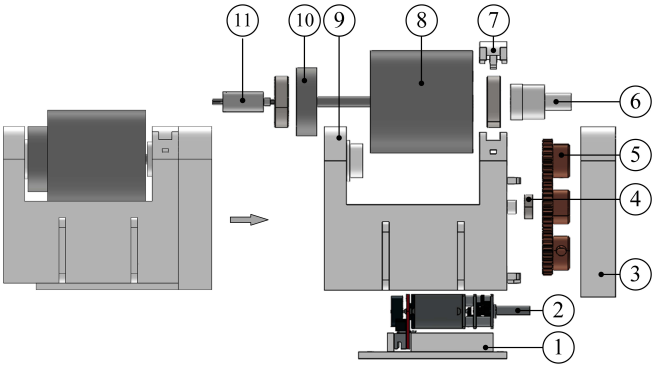

Figure 3. Exploded view of active roller unit. (1) Motor cover, (2) micro DC motor, (3) unit side cover, (4) bearing, (5) gear set, (6) spool connector, (7) bearing cover, (8) active roller, (9) unit body, (10) spool, and (11) slip ring.

The gripper consists of six actuators and a total of 44 parts, most of which are 3D-printed. The dimensions of the gripper are 137 × 153 × 231 mm and the weight is 640 g. The gripper prototype is shown in Figure 4.

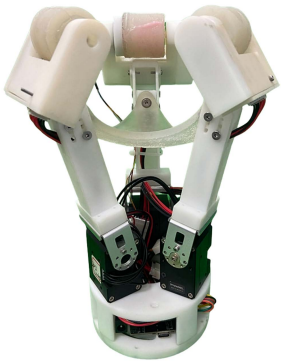

Figure 4. Fabricated gripper prototype.

2.2. Force Sensing Capability

When the gripper comes into contact with the fruit, the active roller is compressed. Assuming that the mass of the air within the roller is constant, the air volume change will lead to a change in the pressure in the roller, which can be further measured by the pressure sensor. The manufacturing of the active roller is divided into two steps (as shown in Figure 5). Hence, the mold is also divided into two parts. At first, the silicone gel with Shore A Hardness 20 is injected slowly into mold 1 to create the main body of the active roller. After the silicone gel is fully cured, mold 1 is removed and the pressure sensor is embedded into the main body of the active roller via a silicone tube with an outer diameter of 4 mm. The wires of the sensor pass through the silicone tube and are connected to the microcontroller. Then, the silicone gel is poured into mold 2, and the main body of the active roller together with the sensor is put into mold 2 to form a sealed space. The fabricated roller is 30 mm in diameter and 30 mm in length. It is worth mentioning that, to obtain good sealing performance, the silicone tube needs to be sealed with silicone gel.

To quantitatively obtain the force–pressure relationship, the roller is calibrated on a force-displacement test bench (as shown in Figure 6). The external force can be slowly applied to the roller by rotating the bench wheel, and the force is recorded in real time using a force gauge (ZTS-50N, IMADA Inc., Toyohashi, Aichi Prefecture, Japan). In the calibration experiment, the initial pressure in the roller was 1044.57 hPa. The calibration experiment was repeated three times, and the average value was computed as the final

result. The calibration result is shown in Figure 7. The force-pressure relationship can be expressed as

$$P = -0.485F^3 + 4.455F^2 + 3.413F + 1044.8, R^2 = 0.9996 \quad (1)$$

where P and F are the pressure and the force. R^2 is the coefficient of determination, which quantifies a goodness of fit.

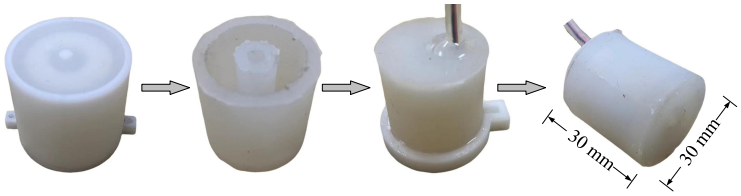

Figure 5. General fabrication process of active roller.

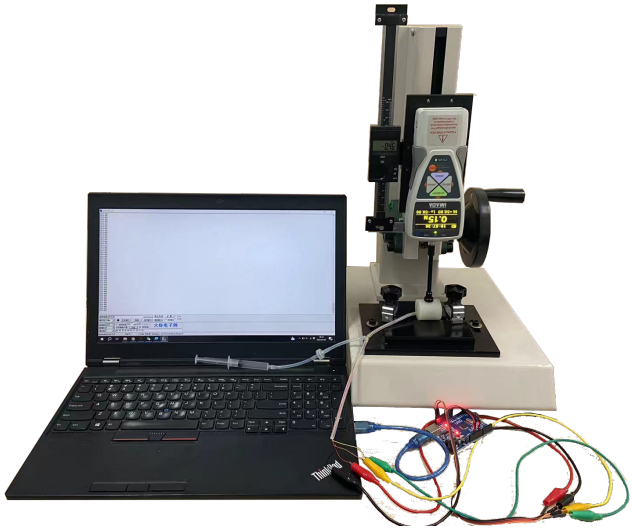

Figure 6. Experimental setup of active roller.

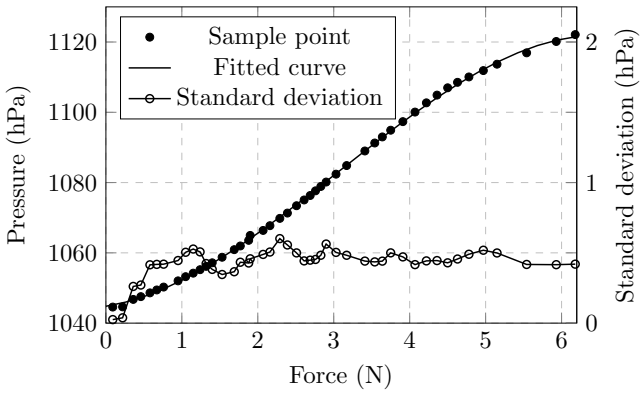

Figure 7. Force–pressure relationship of active roller.

2.3. Gripper–Fruit Interaction Model

The execution steps of the gripper can be divided into three stages (as shown in Figure 8). In the contact stage, the gripper is controlled to apply a gentle touch to the object at a given opening angle. When a touch is detected, the active rollers are activated to rotate at a given speed. Then, the fruit begins to be translated toward the gripper through friction (as shown in Figure 8a). The translation stage follows the contact stage. In this stage, as the fruit translates, the smart actuator is activated to apply a stable desired force to the fruit,

and the opening angle of the gripper gradually increases to facilitate the translation process (as shown in Figure 8b). When the fruit is completely translated in the gripper, the active rollers stop rotating and the smart actuator is locked to impose constraints on the fruit (as shown in Figure 8c).

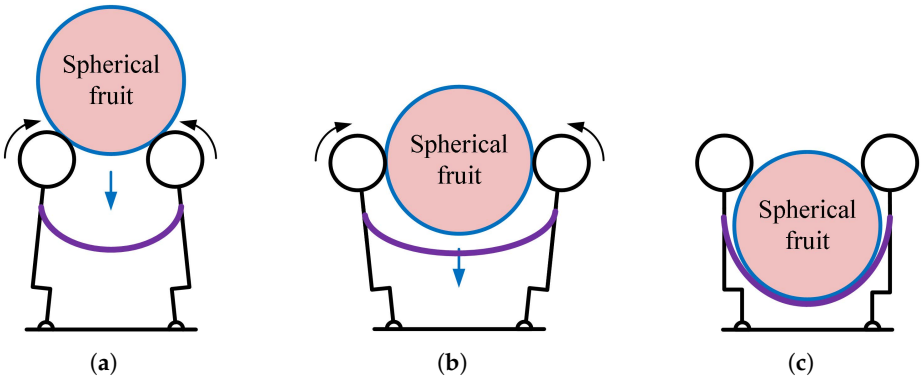

Figure 8. Simplified diagram of three-stage gripper–fruit interaction. (**a**) Fruit contact stage. (**b**) Fruit translation stage. (**c**) Fruit constraint stage.

The cooperation of the links and the active rollers provides the translational force, which has a great influence on whether the fruit can be handled smoothly. This translational force is determined by multiple factors, such as the opening angle of the gripper, the friction coefficient of the roller, and the torque of the smart actuator. The specific force analysis of the single roller on the fruit is displayed in Figure 9. The single roller exerts two forces on the fruit: a normal force F_n and friction force f. F_n can be decomposed into F_{nr} and F_{no} along the translational direction. Similarly, f can be decomposed into f_r and f_i. Assume that the equivalent length of the link is L_a and the radii of the roller and the fruit are R_l and R_g respectively; then, the effect of the single roller on the fruit can be treated as the translational force F_t and the gathering force F_r, which are further expressed as

$$\begin{cases} F_t = f_i - F_{no} = \sin\delta f - \cos\delta F_n \\ F_r = f_r + F_{nr} = \cos\delta f + \sin\delta F_n \end{cases} \tag{2}$$

where δ is the angle between F_{no} and F_n. f can be calculated as $f = \mu_l F_n$, where μ_l is the friction coefficient. Considering the mechanical relationship between the gripper and the fruit, the following equation can be obtained:

$$\sin\delta\left(R_l + R_g\right) = \sin\gamma L_a \tag{3}$$

where γ is the opening angle of the gripper.

It is worth noting that the fruit will be translated toward the gripper only if F_t is greater than zero. Otherwise, F_t behaves as a translational repulsive force, preventing the fruit from being successfully handled. Assume that, when $F_t = 0$, the opening angle of the gripper is the critical angle γ_c. When controlling the gripper to handle fruits of different sizes, γ_c needs to be carefully considered.

F_t and F_r will drive the fruit to move along the translational direction and the gathering direction, respectively (as displayed in Figure 9). Considering a gripper with n uniformly arranged rollers, the resultant force of all gathering forces will be zero and the resultant force of all translational forces is F_T, which can be calculated as $F_T = nF_t$. Assume that the gripper approaches a fruit at a given angle β, which is the angle between the gripper and the horizontal direction. As displayed in Figure 10, the angle β is also the angle between

F_T and the horizontal direction. The following equation can be obtained to successfully handle the fruit:

$$\sin \beta F_T \geq G \tag{4}$$

where G is the fruit gravity. O_0 and O in Figure 10 are the initial position and the current position of the fruit, respectively.

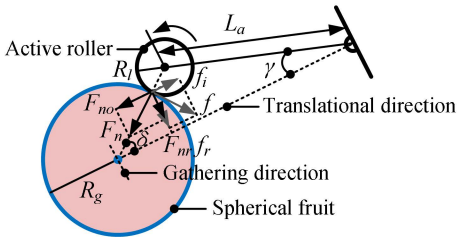

Figure 9. Force analysis of single active roller on fruit.

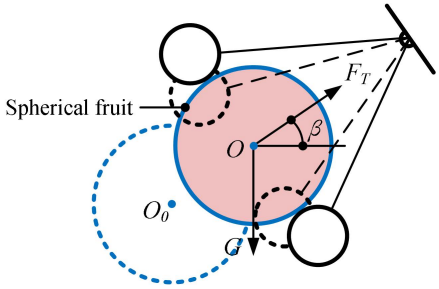

Figure 10. Force analysis of whole gripper during grasping.

3. Gripper Evaluation

To evaluate the effectiveness of the proposed gripper, three experiments were conducted.

3.1. Experiment #1

This experiment aimed to evaluate the gripper handling capability as well as the impact of the roller speed (ω) and the actuator torque (τ) on the gripper performance. The experiment was divided into two rounds.

3.1.1. Experimental Setup and Methods

In the first round, it aimed to determine the maximum graspable weight (GW_{max}) of the gripper under different combinations of ω and τ. As shown in Figure 11, the gripper was mounted at the end of a robotic arm (Z1, Unitree). The target objects used were plastic balls with diameters of 60, 70, and 80 mm, and their weights could be adjusted by filling them with lead pellets. The robotic arm was controlled to move from position A (10 cm directly above the equatorial plane of the target object) to position B, which was the equatorial plane of the target object. The arm then moved back to position A, held for one second, and subsequently returned the target object to position B. To determine GW_{max} for each $\omega - \tau$ pair, a binary search method was employed to incrementally adjust the weight of the ball, until GW_{max} was identified. ω was set at 20, 40, 60, 80, 100, and 120 rpm, while τ was set at 50, 80, 110, 140, 170, and 200 mN·m. The values 20 rpm and 50 mN·m were the minimum values required to drive the gripper, whereas noticeable damage to the tomatoes occurred when ω exceeded 120 rpm or τ exceeded 200 mN·m. GW_{max} was selected as the maximum weight that could be successfully grasped five times for each $\omega - \tau$ pair. A trial was considered successful if the target object was grasped and not dropped.

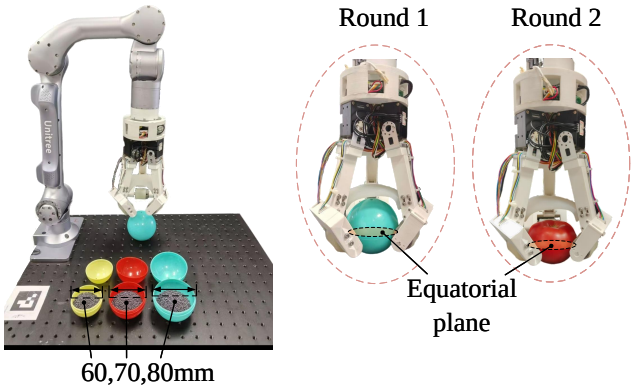

Figure 11. Setup of Experiment #1.

The setup for the second round was almost the same as the first round. However, the target objects were replaced with the tomatoes of three diameter ranges: 55–65 mm, 65–75 mm, and 75–85 mm. Ten tomatoes were used in each diameter range. The focus of the second round was to evaluate the damage rate (d) under different $\omega - \tau$ pairs, thus characterizing the flexibility of the gripper. The damage rate was defined as $d = 1 - \frac{p}{n}$. p represented the number of successful trials without significant dents or visible damage to the surface of the tomato. n was the total number of successful trials. The experimental process for this round remained consistent with the first round, ensuring a joint analysis of GW_{max} and d.

3.1.2. Results and Discussion

The results of Round 1 are shown in Figure 12. Overall, τ has a significant impact on the GW_{max} of the gripper. For a given ω, GW_{max} increases significantly with the increase of τ. In contrast, ω has a relatively weak effect on the GW_{max} of the gripper. For a given τ, the rise of GW_{max} is limited as ω increases. Taking Figure 12b as an example, at a given speed of 60 rpm, the corresponding GW_{max} increases from 167 g at 40 mN·m to 1032 g at 200 mN·m, representing an increase of 518%, while, at a given torque of 110 mN·m, the corresponding GW_{max} increases from 685 g at 20 rpm to 973 g at 120 rpm, showing an increase of only 42%. As shown in Figure 12a–c, for the plastic balls with diameters of 60 mm, 70 mm, and 80 mm, the corresponding maximum GW_{max} values all occur at 120 rpm–200 mN·m, reaching 662 g, 1038 g, and 2077 g, respectively.

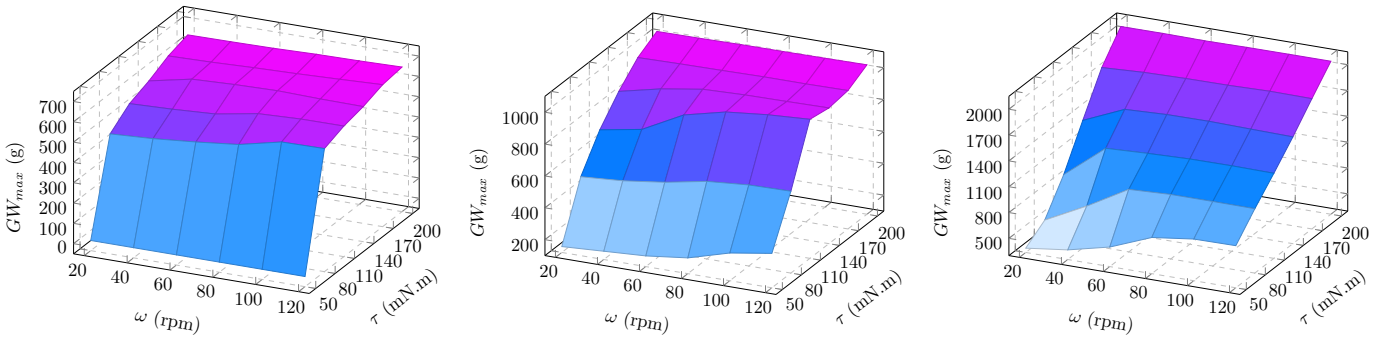

Figure 12. GW_{max} of gripper at 36 $\omega - \tau$ pairs. (**a**) Blue ball with diameter of 60 mm. (**b**) Red ball with diameter of 70 mm. (**c**) Yellow ball with diameter of 80 mm.

The results of Round 2 are shown in Figure 13. Based on the data in Figure 13a–c, beyond certain limits, d shows an obvious upward trend with the increase of both ω and τ. When handling tomatoes with a diameter of 55–65 mm (as displayed in Figure 13a), at the roller speed of 80 rpm, the corresponding d is 0% at 50, 80, 110, and 140 mN·m, then increases to 12% at 170 mN·m, and finally reaches the maximum value of 32% at 200 mN·m. At the actuator torque of 140 mN·m, the corresponding d is 0% at 20, 40, 60, and 80 rpm, then increases to 8% at 100 rpm, and finally reaches the maximum value of 16% at 120 rpm. The $\omega - \tau$ pair limit between $d = 0$ and $d \neq 0$ is 120 rpm–50 mN·m, 100 rpm–80 mN·m, 80 rpm–110 mN·m, 80 rpm–140 mN·m, 60 rpm–170 mN·m, and 40 rpm–200 mN·m. Similarly, the $\omega - \tau$ pair limit in Figure 13b is 100 rpm–50 mN·m, 80 rpm–80 mN·m, 60 rpm–110 mN·m, 40 rpm–140 mN·m, and 20 rpm–170 mN·m. Figure 13c has the $\omega - \tau$ pair limit of 80 rpm–50 mN·m, 60 rpm–80 mN·m, 40 rpm–110 mN·m, and 20 rpm–110 mN·m. At 120 rpm-200 mN·m, the maximum d values of the tomatoes with diameters of 55–65 mm, 65–75 mm, and 75–85 mm are 36%, 40%, and 68%, respectively. In addition, some outliers are observed during the experiment, such as the d of tomatoes with a diameter of 55–65 mm at 120 rpm–80 mN·m and 100 rpm–110 mN·m, and the d of tomatoes with a diameter of 65–75 mm at 60 rpm–200 mN·m. This might be due to the instability of the output torque caused by the long-term operation of the smart actuator.

Although increasing ω and τ enhances the handling capability, it also significantly increases the damage to the tomatoes, particularly for the tomatoes with a larger diameter. Therefore, to balance handling capability and flexibility, it is essential to identify an appropriate combination of ω and τ to achieve optimal values for both GW_{max} and d. It can be seen that the GW_{max} of most of the plastic balls in Figure 12 is much higher than the mass of the tomatoes in Figure 13, indicating that excessively high GW_{max} does not significantly help in handling tomatoes. To maximize handling capability while ensuring flexibility, the $\omega - \tau$ pairs with $d = 0$ were selected and the GW_{max} sum of the same $\omega - \tau$ pair across the three diameter groups was calculated. As shown in Figure 14, the 40 rpm–110 mN·m pair has the highest total GW_{max}.

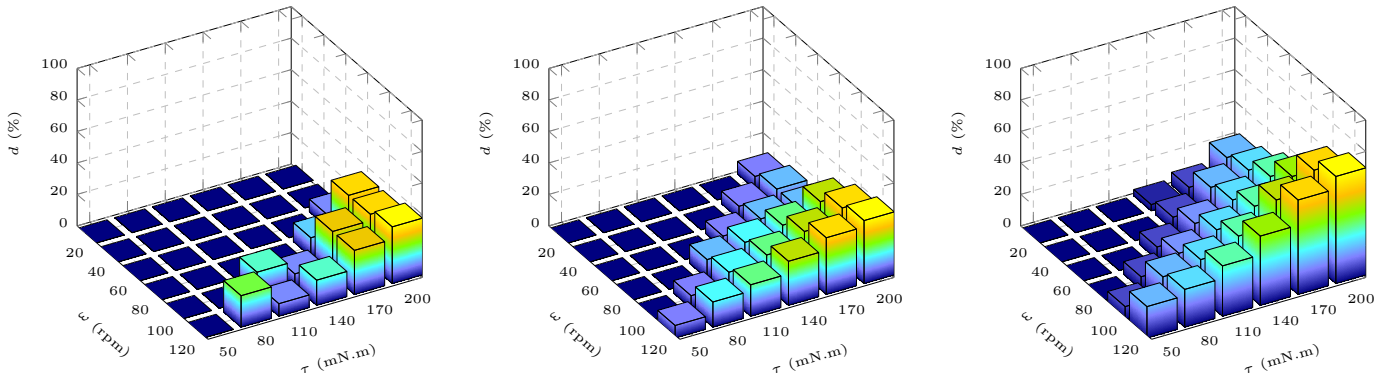

Figure 13. d of gripper at 36 $\omega - \tau$ pairs. (**a**) Tomatoes with a diameter of 55–65 mm. (**b**) Tomatoes with a diameter of 65–75 mm. (**c**) Tomatoes with a diameter of 75–85 mm.

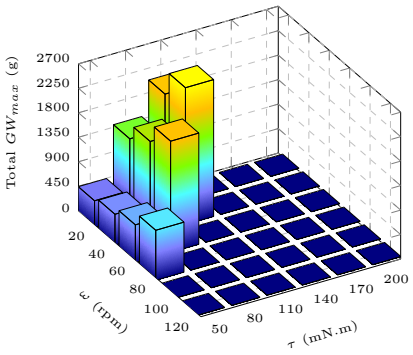

Figure 14. Total GW_{max} under $d = 0$ at 36 $\omega - \tau$ pairs.

3.2. Experiment #2

The purpose of this experiment was to evaluate the tolerance of the gripper to positional offset when handling tomatoes.

3.2.1. Experimental Setup and Methods

The task involved using the proposed gripper to grasp tomatoes under different offset values and recording the failure rate of the experimental attempts. This experiment was divided into three rounds and 30 tomatoes with a diameter range of 55–85 mm were selected as the target objects in each round. Considering the results in Experiment #1, the roller speed (ω) and the actuator torque (τ) of the gripper were set to 40 rpm and 110 mN·m, respectively, in all three rounds.

As shown in Figure 15, the gripper is controlled to grasp the tomatoes at different vertical offsets in the first round. The specific vertical offset values were 0, 3, 6, 9, 12, and 15 mm. The vertical offset of 0 mm indicated that the gripper applied contact to the equatorial plane of the tomato. The other vertical offset values (3, 6, 9, 12, and 15 mm) indicated that the gripper contact plane was shifted vertically upward from the equatorial plane by these set values. The number of no-fall trials (s) and the number of total trials (m) were recorded in this round. Then, the failure rate $f = 1 - s/m$ was calculated.

In the second round, the gripper was controlled to grasp the tomatoes at different horizontal offsets and the specific horizontal offset values were 0, 3, 6, 9, 12, and 15 mm. Similarly, the horizontal offset of 0 mm indicated that the gripper applied contact to the equatorial plane of the tomato, while the other horizontal offset values (3, 6, 9, 12, and 15 mm) represented that the gripper contact plane was shifted horizontally from the equatorial plane by these set values.

In the last round, the gripper was controlled to grasp the tomatoes at the offsets in both vertical and horizontal directions, and the offset values of each unilateral direction were still 0, 3, 6, 9, 12, and 15 mm, forming a total of 36 pairs.

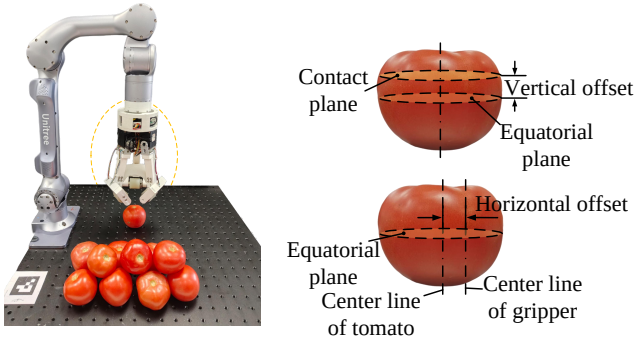

Figure 15. Setup of Experiment #2.

3.2.2. Results and Discussion

The failure rate data at the unilateral direction of the three rounds are calculated in Figure 16.

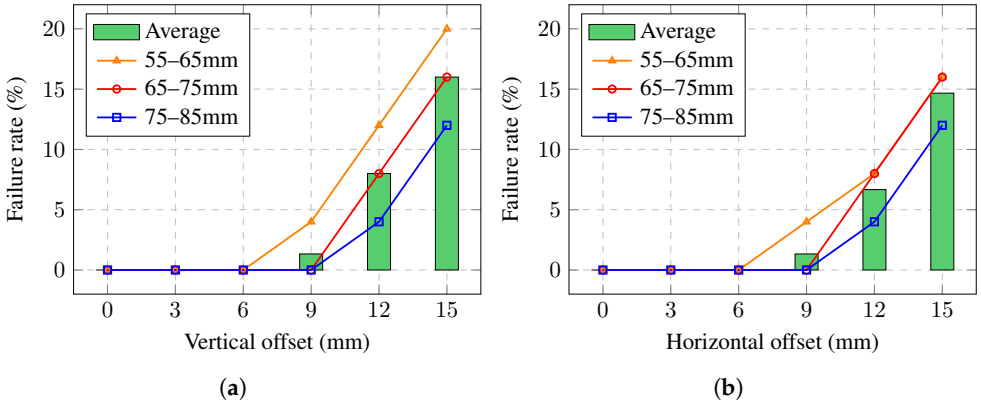

(**a**) (**b**)

Figure 16. Failure rate at unilateral direction. (**a**) Failure rate at vertical offsets. (**b**) Failure rate at horizontal offsets.

In the first round (displayed in Figure 16a), the failure rate shows an overall upward trend as the vertical offset increases. At the vertical offsets of 0, 3, and 6 mm, the failure rate is 0 for all three diameter ranges. The failure rate of the tomatoes within 65–75 mm and 75–85 mm diameter at 9 mm vertical offset is still 0, and that within 55–65 mm diameter is 4%, having an average failure rate of only 1.33%. When the vertical offset increases to 12 mm and 15 mm, the average failure rate is calculated to be 8% and 16%, respectively. The reason for the increase in the failure rate is that, as the vertical offset increases, F_t decreases, which leads to a rise in the failure rate. As shown in Figure 16b, there is a similar trend in the failure rate at the horizontal offset. When the horizontal offset is 0, 3, and 6 mm, the failure rate is still 0% in all three diameter ranges. The average failure rate for the horizontal offset of 9 mm is only 1.33%, which is the same as the average failure rate for the same offset in the vertical direction. When the horizontal offset increases to 12 mm and 15 mm, the average failure rates are 6.67% and 14.67%, respectively, which are slightly lower than those values in the vertical direction. The increase in the failure rate is due to the fact that, when the horizontal offset becomes too large, the gripper is inadequate to gather the tomato toward the central position, leading to handling failure. Therefore, the gripper has a relatively high positional offset tolerance, and the average failure rate is less than 10% when the offset reaches 12 mm in the two unilateral directions. Moreover, the gripper performs better at the horizontal offsets than at the vertical offsets. It is worth pointing out that, at the same vertical offset, the failure rate was observed to decrease as the tomato diameter increased gradually. This could be explained by Equation (2): when the vertical offset was the same, the tomato with a larger diameter had a larger δ, and thus a larger F_t.

The gripper performance deteriorates when the positional offsets in the bilateral directions are applied (shown in Figure 17). As shown in Figure 17a, the failure rate gradually increases with the increase of the offset pairs. The boundaries of the horizontal–vertical offset pairs between $f = 0$ and $f \neq 0$ within 55–65 mm diameter are 0–6 mm, 3–6 mm, 6–3 mm, and 6–0 mm. Similarly, the boundaries within 65–75 mm diameter are 0–9 mm, 3–6 mm, 6–6 mm, 9–3 mm, and 9–0 mm (shown in Figure 17b), and, within 75–85 mm diameter, are 0–9 mm, 3–9 mm, 6–9 mm, 9–6 mm, 9–3 mm, and 9–0 mm (shown in Figure 17c). At the 6–6 mm and 9–9 mm pair, the gripper has the average failure rate of 4% and 18.67%, respectively, larger than 0% and 1.33% in the unilateral direction. At the 15–15 mm pair, the maximum failure rate values within the diameters of 55–65 mm, 65–75 mm, and 75–85 mm reaches 68%, 72%, and 52%, respectively. Overall, although the

performance of the gripper deteriorates in the bilateral directions, the failure rate is still less than 20% at 9–9 mm offset pair.

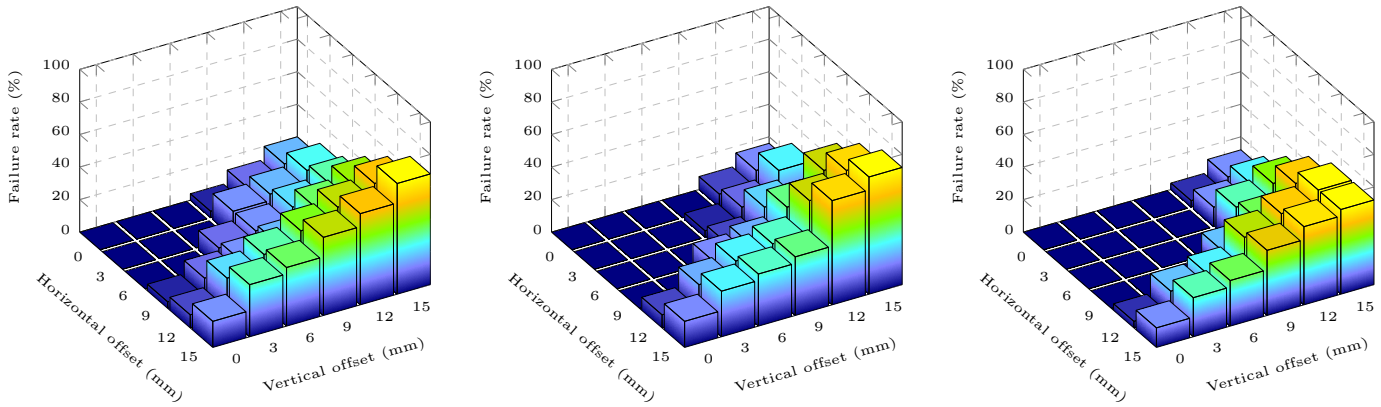

Figure 17. Failure rate of gripper at 36 horizontal–vertical offset pairs. (**a**) Tomatoes with a diameter of 55–65 mm. (**b**) Tomatoes with a diameter of 65–75 mm. (**c**)Tomatoes with a diameter of 75–85 mm.

3.3. Experiment #3

This experiment aimed to verify the effectiveness of the proposed gripper for tomato-picking in a simplified laboratory scenario.

3.3.1. Experimental Setup and Methods

As displayed in Figure 18a, the proposed gripper is attached to the robotic arm. The tomatoes with branches are fixed on a frame. The task was to control the robotic arm and the gripper to pick the tomatoes from the branches. The control process of the robot arm based on the depth camera is shown in Figure 19. A depth camera (D435, Intel RealSense) was used to capture the images and depth information. The position of the tomato was determined by YOLOv8 and Intel RealSense SDK 2.0. Then, a coordinate transformation was performed to convert the camera coordinates into the robot arm coordinates. After that, the robot arm was controlled by the Unitree SDK so that the gripper contacted the surface of the tomato (as shown in Figure 18b). Then, the gripper was activated and the tomato was translated toward the gripper. When the tomato was picked into the gripper, the fingers of the gripper were locked and the robotic arm was controlled to move backward to detach the tomato from the branch. A controller was utilized to maintain compliance (shown in Figure 20). In the compliance controller, a PID controller was used in the motion control to drive the three links of the gripper to the desired trajectories θ_i^d, $i = 1, 2, 3$ at the same time. The real angles and angular velocities of the links were measured by the encoders. Considering that ripe tomatoes are usually soft, an impedance controller was introduced as a feed-forward of the motion control to adjust the velocity of the end of each link. The actual force between the gripper and the tomato was given by the pressure sensor; hence, the gripper picked the fruit with the appropriate force according to the adjusted angular velocity. Considering the constraint between the tomato and the branch, the gripper was controlled to apply 6 N force to the tomato and the roller speed was set at 120 rpm. During the experiment, the success and damage rates were recorded to evaluate the picking performance. After the experiment, the diameter and number of tomatoes were measured.

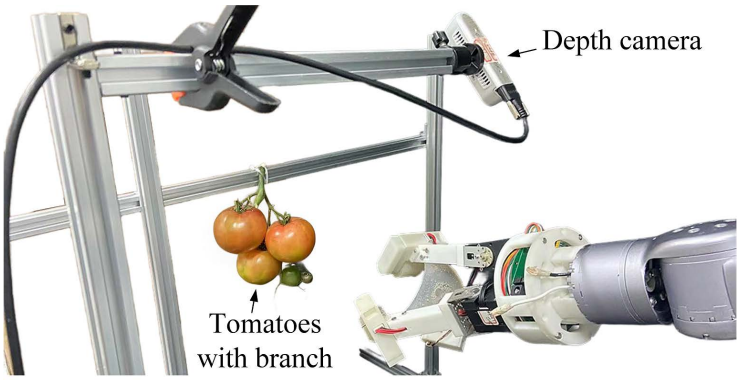

(**a**)

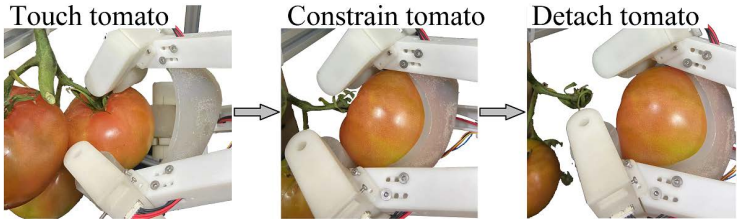

(**b**)

Figure 18. Setup of proposed gripper in Experiment #3. (**a**) Tomato-picking task in simplified laboratory scenario. (**b**) Three main steps in tomato-picking task.

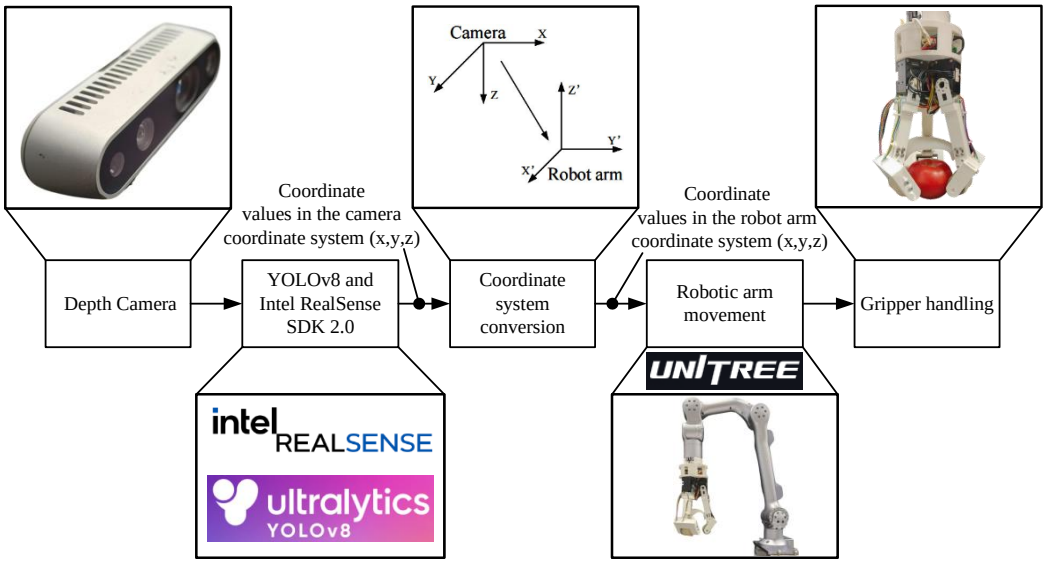

Figure 19. The robotic arm control flow chart based on the depth camera.

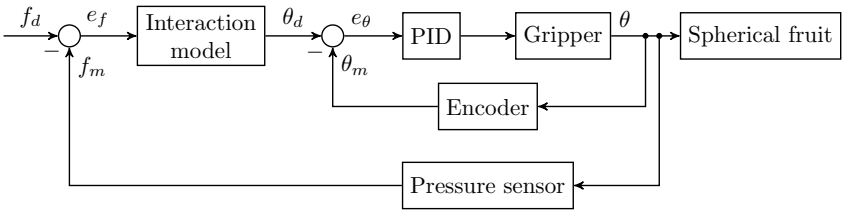

Figure 20. Compliance control diagram of gripper. θ_d, θ_m, and θ are desired, measured, and actual angles of link, respectively. e_θ is angle error. f_d and f_m are desired and measured forces. e_f is force error.

3.3.2. Results and Discussion

The typical interaction force recorded in the experiment is shown in Figure 21. In the contact stage, a small fluctuating force is recorded, which could be due to the non-smooth surface of the roller. Then, as the fruit is translated, the force steadily increases until it reaches the set value and remains within a certain range. When the fruit is completely constrained, the force gradually drops.

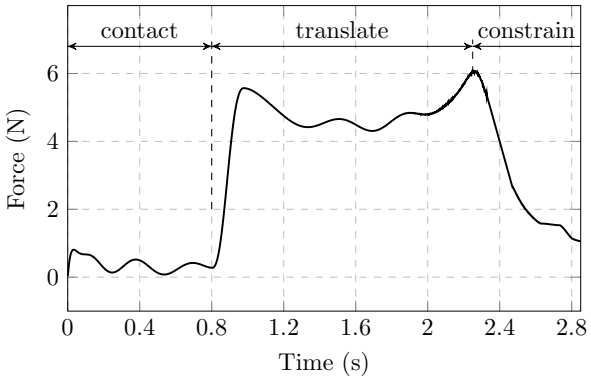

Figure 21. Typical interaction force recorded in Experiment #3.

A total of 56 tomatoes with four diameter ranges were recorded in this experiment. The experimental results (shown in Table 2) indicate the average success rate is 0.874, which is close to Experiment #2 Round 1 (0.876). Before being completely translated into the gripper, four tomatoes were observed detaching from the branches and falling onto the table. This showed that the constraints between tomatoes and branches were not completely secure after transportation from the greenhouse to the laboratory. Three tomatoes were not successfully detached from the branches, possibly due to differences in tomato maturity. In addition, three tomatoes were observed to be damaged. The average damage rate was calculated to be 0.064. There were two reasons: (1) the picking attempts were inadequate, and (2) a large force was applied to the tomato to break the binding force between the tomato and the branch.

Table 2. Results of Experiment #3.

Size (mm)	Number	Success Rate	Damage Rate
80–90	12	0.833	0.100
70–80	15	0.866	0
60–70	17	0.882	0.067
50–60	12	0.916	0.091
Average	-	0.874	0.064

4. Conclusions

The design, analysis, and evaluation of an active roller gripper for spherical fruit handling were presented in this paper. Its mechanical design, force sensing capabilities, gripper–fruit interaction model, and evaluation experiments were sequentially demonstrated. The gripper mainly includes a base, a control unit, a soft membrane, and three fingers. Each finger comprises a smart actuator, a link, and an active roller unit. When in contact with the fruit, the smart actuator applies force to it, and the active roller rotates at a given speed. Then, the fruit can be translated into the gripper through the frictional force, achieving low damage rates and stable handling of the fruit. The pressure sensor embedded in the active roller is used for force measurement, which greatly improves the gripper's compliance. To verify the effectiveness of the proposed gripper, three experi-

ments were designed and conducted. Experiment #1 consisted of two rounds and was designed to evaluate the gripper's handling capabilities and the effects of roller speed (ω) and actuator torque (τ) on the gripper's performance. The results of the first and second rounds indicated that GW_{max} showed a clear upward trend with the increase of τ, while the increase of GW_{max} was limited as ω increased. For the plastic balls with diameters of 60, 70, and 80 mm, GW_{max} was 662, 1038, and 2077 g, respectively. Experiment #2 was designed to verify the gripper's tolerance to positional offsets. The results showed that when the vertical offset and horizontal offset were 12 mm, the average failure rates were 8% and 6.67%, respectively. The average failure rate was only 4% at the bilateral offset of 6-6 mm. Experiment #3 was designed to verify the gripper's picking performance in a simplified laboratory scenario. The proposed gripper could achieve an average success rate of 0.874 and an average damage rate of 0.064.

Future work includes (1) testing and calibrating the pressure sensor in the active roller to provide accurate and consistent force under different environmental conditions, (2) optimizing the silicone membrane to balance flexibility and durability for different fruit types, (3) using silicone materials with a higher coefficient of friction to achieve higher positional offset tolerance, and (4) conducting experiments in more complex branch arrangements or clustered fruit scenarios to verify the actual performance of the gripper.

Author Contributions: Conceptualization, H.Q., Z.Q., and H.Z.; methodology, H.Q.; software, Z.Q.; validation, H.Z., Z.Q., and H.Q.; formal analysis, J.X.; investigation, H.Z. and H.Q.; resources, H.Q. and M.L.; data curation, H.Z.; writing—original draft preparation, H.Q. and H.Z.; writing—review and editing, X.C., J.X., X.G., and M.L.; visualization, not applicable; supervision, not applicable; project administration, H.Q. and X.G.; funding acquisition, X.C. and H.Q. All authors have read and agreed to the published version of the manuscript.

Funding: This research was funded by the Natural Science Foundation of Jiangsu Province (Grant No. BK20210408) and the Key Research and Development Plan Projects in Xinjiang Autonomous Region (Grant No. 2022B02027-1).

Institutional Review Board Statement: Not applicable.

Informed Consent Statement: Not applicable.

Data Availability Statement: The raw data supporting the conclusions of this article will be made available by the authors on request.

Conflicts of Interest: The funders had no role in the design of the study; in the collection, analyses, or interpretation of data; in the writing of the manuscript; or in the decision to publish the results.

References

1. Oguntibeju, O.; Truter, E.; Esterhuyse, A. The role of fruit and vegetable consumption in human health and disease prevention. *Diabetes Mellit.-Insights Perspect.* **2013**, *3*, 172–180.
2. Zhou, H.; Wang, X.; Au, W.; Kang, H.; Chen, C. Intelligent robots for fruit harvesting: Recent developments and future challenges. *Precis. Agric.* **2022**, *23*, 1856–1907. [CrossRef]
3. Ren, X.; Huang, B.; Yin, H. A review of the large-scale application of autonomous mobility of agricultural platform. *Comput. Electron. Agric.* **2023**, *206*, 107628. [CrossRef]
4. Oliveira, L.F.; Moreira, A.P.; Silva, M.F. Advances in agriculture robotics: A state-of-the-art review and challenges ahead. *Robotics* **2021**, *10*, 52. [CrossRef]
5. Birrell, S.; Hughes, J.; Cai, J.Y.; Iida, F. A field-tested robotic harvesting system for iceberg lettuce. *J. Field Robot.* **2020**, *37*, 225–245. [CrossRef]
6. Droukas, L.; Doulgeri, Z.; Tsakiridis, N.L.; Triantafyllou, D.; Kleitsiotis, I.; Mariolis, I.; Giakoumis, D.; Tzovaras, D.; Kateris, D.; Bochtis, D. A Survey of Robotic Harvesting Systems and Enabling Technologies. *J. Intell. Robot. Syst.* **2023**, *107*, 21. [CrossRef] [PubMed]

7. Au, W.; Zhou, H.; Liu, T.; Kok, E.; Wang, X.; Wang, M.; Chen, C. The Monash Apple Retrieving System: A review on system intelligence and apple harvesting performance. *Comput. Electron. Agric.* **2023**, *213*, 108164. [CrossRef]
8. Li, Z.; Yuan, X.; Wang, C. A review on structural development and recognition–localization methods for end-effector of fruit–vegetable picking robots. *Int. J. Adv. Robot. Syst.* **2022**, *19*, 17298806221104906. [CrossRef]
9. Kakogawa, A.; Kaizu, Y.; Ma, S. Sensor-Less and Control-Less Underactuated Grippers With Pull-In Mechanisms for Grasping Various Objects. *Front. Robot. AI* **2021**, *8*, 631242. [CrossRef]
10. Yuan, S.; Shao, L.; Yako, C.L.; Gruebele, A.; Salisbury, J.K. Design and control of roller grasper v2 for in-hand manipulation. In Proceedings of the 2020 IEEE/RSJ International Conference on Intelligent Robots and Systems (IROS), Las Vegas, NV, USA, 24 October 2020–24 January 2021; pp. 9151–9158.
11. Zhang, B.; Xie, Y.; Zhou, J.; Wang, K.; Zhang, Z. State-of-the-art robotic grippers, grasping and control strategies, as well as their applications in agricultural robots: A review. *Comput. Electron. Agric.* **2020**, *177*, 105694. [CrossRef]
12. Liu, C.H.; Chiu, C.H.; Chen, T.L.; Pai, T.Y.; Chen, Y.; Hsu, M.C. A soft robotic gripper module with 3D printed compliant fingers for grasping fruits. In Proceedings of the 2018 IEEE/ASME International Conference on Advanced Intelligent Mechatronics (AIM), Auckland, New Zealand, 9–12 July 2018; pp. 736–741.
13. Russo, M.; Ceccarelli, M.; Corves, B.; Hüsing, M.; Lorenz, M.; Cafolla, D.; Carbone, G. Design and test of a gripper prototype for horticulture products. *Robot. Comput.-Integr. Manuf.* **2017**, *44*, 266–275. [CrossRef]
14. Silwal, A.; Davidson, J.R.; Karkee, M.; Mo, C.; Zhang, Q.; Lewis, K. Design, integration, and field evaluation of a robotic apple harvester. *J. Field Robot.* **2017**, *34*, 1140–1159. [CrossRef]
15. Yaguchi, H.; Nagahama, K.; Hasegawa, T.; Inaba, M. Development of an autonomous tomato harvesting robot with rotational plucking gripper. In Proceedings of the 2016 IEEE/RSJ international conference on intelligent robots and systems (IROS), Daejeon, Republic of Korea, 9–14 October 2016; pp. 652–657.
16. Zhou, S.; Li, Y.; Wang, Q.; Lyu, Z. Integrated Actuation and Sensing: Toward Intelligent Soft Robots. *Cyborg Bionic Syst.* **2024**, *5*, 0105. [CrossRef] [PubMed]
17. Zhang, Z.; Fan, W.; Long, Y.; Dai, J.; Luo, J.; Tang, S.; Lu, Q.; Wang, X.; Wang, H.; Chen, G. Hybrid-Driven Origami Gripper with Variable Stiffness and Finger Length. *Cyborg Bionic Syst.* **2024**, *5*, 0103. [CrossRef] [PubMed]
18. Yuan, S.; Epps, A.D.; Nowak, J.B.; Salisbury, J.K. Design of a roller-based dexterous hand for object grasping and within-hand manipulation. In Proceedings of the 2020 IEEE International Conference on Robotics and Automation (ICRA), Paris, France, 31 May–31 August 2020; pp. 8870–8876.
19. Ma, R.R.; Dollar, A.M. In-hand manipulation primitives for a minimal, underactuated gripper with active surfaces. In *International Design Engineering Technical Conferences and Computers and Information in Engineering Conference*; American Society of Mechanical Engineers: New York, NY, USA, 2016 ; Volume 50152, p. V05AT07A072.
20. Vita Ostuni, B.M.; Grazioso, S.; Caporaso, T.; Lanzotti, A. Design and Testing of a Single-Tentacle Soft Gripper with an Embedded Suction Cup. *Procedia CIRP* **2024**, *125*, 337–342. [CrossRef]
21. Hohimer, C.J.; Wang, H.; Bhusal, S.; Miller, J.; Mo, C.; Karkee, M. Design and field evaluation of a robotic apple harvesting system with a 3D-printed soft-robotic end-effector. *Trans. ASABE* **2019**, *62*, 405–414. [CrossRef]
22. Xie, M.; Zhu, M.; Yang, Z.; Okada, S.; Kawamura, S. Flexible self-powered multifunctional sensor for stiffness-tunable soft robotic gripper by multimaterial 3D printing. *Nano Energy* **2021**, *79*, 105438. [CrossRef]
23. Wang, Z.; Or, K.; Hirai, S. A dual-mode soft gripper for food packaging. *Robot. Auton. Syst.* **2020**, *125*, 103427. [CrossRef]
24. Park, W.; Seo, S.; Bae, J. A hybrid gripper with soft material and rigid structures. *IEEE Robot. Autom. Lett.* **2018**, *4*, 65–72. [CrossRef]
25. Chen, K.; Li, T.; Yan, T.; Xie, F.; Feng, Q.; Zhu, Q.; Zhao, C. A soft gripper design for apple harvesting with force feedback and fruit slip detection. *Agriculture* **2022**, *12*, 1802. [CrossRef]
26. Shintake, J.; Cacucciolo, V.; Floreano, D.; Shea, H. Soft robotic grippers. *Adv. Mater.* **2018**, *30*, 1707035. [CrossRef] [PubMed]
27. Jo, Y.; Park, Y.; Son, H.I. A suction cup-based soft robotic gripper for cucumber harvesting: Design and validation. *Biosyst. Eng.* **2024**, *238*, 143–156. [CrossRef]
28. Koivikko, A.; Drotlef, D.M.; Dayan, C.B.; Sariola, V.; Sitti, M. 3D-Printed Pneumatically Controlled Soft Suction Cups for Gripping Fragile, Small, and Rough Objects. *Adv. Intell. Syst.* **2021**, *3*, 2100034. [CrossRef]
29. Krahn, J.M.; Fabbro, F.; Menon, C. A soft-touch gripper for grasping delicate objects. *IEEE/ASME Trans. Mechatronics* **2017**, *22*, 1276–1286. [CrossRef]
30. Li, S.; Stampfli, J.J.; Xu, H.J.; Malkin, E.; Diaz, E.V.; Rus, D.; Wood, R.J. A vacuum-driven origami "magic-ball" soft gripper. In Proceedings of the 2019 International Conference on Robotics and Automation (ICRA), Montreal, QC, Canada, 20–24 May 2019; pp. 7401–7408.
31. Song, S.; Drotlef, D.M.; Son, D.; Koivikko, A.; Sitti, M. Adaptive Self-Sealing Suction-Based Soft Robotic Gripper. *Adv. Sci.* **2021**, *8*, 2100641. [CrossRef] [PubMed]

32. D'Avella, S.; Sundaram, A.M.; Friedl, W.; Tripicchio, P.; Roa, M.A. Multimodal Grasp Planner for Hybrid Grippers in Cluttered Scenes. *IEEE Robot. Autom. Lett.* **2023**, *8*, 2030–2037. [CrossRef]
33. Shea, H.; Shintake, J.; Floreano, D. *Soft Compliant Gripper for Safe Manipulation of Extremely Fragile Objects*; Technical Report; Springer Nature: Lausanne, Switzerland, 2016.
34. Pettersson, A.; Davis, S.; Gray, J.O.; Dodd, T.J.; Ohlsson, T. Design of a magnetorheological robot gripper for handling of delicate food products with varying shapes. *J. Food Eng.* **2010**, *98*, 332–338. [CrossRef]
35. Tsugami, Y.; Barbié, T.; Tadakuma, K.; Nishida, T. Development of universal parallel gripper using reformed magnetorheological fluid. In Proceedings of the 2017 11th Asian control conference (ASCC), Gold Coast, Australia, 17–20 December 2017; pp. 778–783.
36. Cacucciolo, V.; Shea, H.; Carbone, G. Peeling in electroadhesion soft grippers. *Extrem. Mech. Lett.* **2022**, *50*, 101529. [CrossRef]
37. Sîrbu, I.D.; Bolignari, M.; D'Avella, S.; Damiani, F.; Agostini, L.; Tripicchio, P.; Vertechy, R.; Pancheri, L.; Fontana, M. Adhesion State Estimation for Electrostatic Gripper Based on Online Capacitance Measure. *Actuators* **2022**, *11*, 283. [CrossRef]
38. Hu, F.; Liu, Y. A magneto-elastica reinforced elastomer makes soft robotic grippers. *Sens. Actuators A Phys.* **2024**, *379*, 115977. [CrossRef]